The Flatland Boundary Layer Experiments

Wayne M. Angevine,* Alison W. Grimsdell,* Leslie M. Hartten,* and A. C. Delany+

ABSTRACT

This article describes the 1995 and 1996 Flatland boundary layer experiments, known as Flatland95 and Flatland96. A number of scientific and instrumental objectives were organized around the central theme of characterization of the convective boundary layer, especially the boundary layer top and entrainment zone. In this article the authors describe the objectives and physical setting of the experiments, which took place in the area near the Flatland Atmospheric Observatory, near Champaign–Urbana, Illinois, in August–September 1995 and June–August 1996. The site is interesting because it is extremely flat, has uniform land use, and is in a prime agricultural area. The instruments used and their performance are also discussed. The primary instruments were a triangle of UHF wind-profiling radars. Rawinsondes and surface meteorological and flux instruments were also included. Finally, some early results in terms of statistics and several case studies are presented.

1. Introduction

The continental convective atmospheric boundary layer has been the subject of several experiments over the past decades, but some processes still remain poorly understood. It is also useful to add another site and set of conditions to those previously studied. For these reasons, we undertook two experimental campaigns called Flatland95 and Flatland96. The experiments were conducted in the summers of 1995 and 1996 at and near the Flatland Atmospheric Observatory (FAO), a National Oceanic and Atmosphonic Administration/National Science Foundation (NOAA/NSF) facility near Champaign–Urbana, Illinois. The site is interesting because it is extraordinarily flat, has uniform land use, and is situated in a prime agricultural area.

The objectives of the Flatland experiments fall into two broad categories, scientific and instrumental. The primary scientific objectives focused on the boundary layer top and entrainment zone. The behavior of the entrainment zone at the top of a convective boundary layer is one of the least well-understood phenomena in boundary layer meteorology. It is also very important for modeling and interpreting the dynamics and chemistry of the boundary layer. Measurements of the entrainment zone are difficult to make due to the time and space scales involved. Key quantities are the fluxes of heat and moisture through the boundary layer top (the entrainment fluxes) and the entrainment velocity, defined as the rate at which air from the overlying free troposphere is incorporated into the convective boundary layer. The entrainment velocity is

$$w_e = \frac{d(z_i)}{dt} - w, \tag{1}$$

where z_i is the usual notation for the top of the convective boundary layer, w is the vertical velocity at z_i, defined as positive upward, and horizontal advection of z_i is neglected. In other words, air may be entrained by the increase of the boundary layer height or by moving downward into the boundary layer. Entrainment fluxes of heat, moisture, and chemical species are often a significant fraction of surface fluxes, and may even dominate surface fluxes, especially in the case of moisture. Entrainment controls the mixing of el-

*CIRES, University of Colorado, and NOAA Aeronomy Laboratory, Boulder, Colorado.
+National Center for Atmospheric Research, Boulder, Colorado.
Corresponding author address: Wayne M. Angevine, CIRES, NOAA Aeronomy Laboratory R/E/AL3, Boulder, CO 80303.
In final form 4 November 1997.

evated layers of urban pollutants with locally produced chemical species to produce ozone in the southeastern United States (Trainer et al. 1995). Entrainment parameters have been estimated previously by budget methods using series of radiosondes (e.g., Betts and Barr 1996; Barr and Betts 1998) or aircraft flights (Betts et al. 1992; Grossman 1992; Davis et al. 1998).

The primary scientific objective was to estimate entrainment fluxes and entrainment velocity by several methods. Subsidiary objectives were to measure several terms of the boundary layer heat budget, characterize the thickness and time evolution of the entrainment zone, and examine the effects of boundary layer clouds.

The major instrumental and technique objectives were to examine profiler vertical velocity measurements, both direct and from divergence of the vertical wind over the triangle, and to compare turbulent heat flux measurement techniques (similarity, eddy correlation, conditional sampling) using profiler data.

Previous boundary layer studies have been large-scale projects with aircraft and large networks of surface instrumentation. The Flatland experiments were on a smaller scale and used remote sensing instruments, specifically the 915-MHz lower-tropospheric wind-profiling radar (often called a boundary layer wind profiler). We focused on a relatively small region with well-defined characteristics that allow us to make simplifying assumptions with confidence.

Time and space scales are important considerations in measuring and interpreting boundary layer processes. On the spatial and temporal scale of individual large eddies or thermals (~1 km and ~10 min), the boundary layer height varies greatly, as much as 40% (Stull 1988). On this very small scale, entrainment takes place by the episodic action of overshooting thermals. There are also spatial variations on local, regional, and larger scales, and temporal variations on diurnal, synoptic, and seasonal scales. Divergence, and therefore vertical velocity, varies in a roughly linear way with scale (Young and Eloranta 1995). Vertical velocities in individual thermals and downdrafts are of order 1 m s^{-1}, but on very large scales the vertical velocity is 100 times smaller and may be negligible. In this study, we are interested in a spatial scale of 5–10 km horizontally. On this scale, the terrain within the measurement area is quite flat and the land use uniform, so we do not expect significant variations in boundary layer height over the area.

Two experimental campaigns were conducted. The primary reason for this was to increase our chances of getting sufficient good data in case of bad or anomalous weather or in case the initial experiment design had major flaws. As it turned out, both campaigns yielded much good data. The Flatland95 experiment was 2 months long, from 1 August through 30 September 1995. Some refinements were made to the experiment design for the second campaign, Flatland96, which took place from 15 June to 23 August 1996. Three surface flux measurement systems [Flux-PAM (Portable Automated Mesonet)] were added to the instrument complement for the 1996 campaign.

The wind profiler triangle was the foundation of the experiment. Three boundary layer wind profilers were arranged in a triangle with sides of 5.7, 7.5, and 7.6 km (Fig. 1). selecting the size of the triangle involves tradeoffs between quantifiable and unquantifiable uncertainties. A larger triangle would necessarily include more heterogeneous terrain and land use, and the results might be more contaminated with mesoscale phenomena.

The triangle was located in very flat terrain southwest of Champaign–Urbana, Illinois. One vertex of the triangle was the FAO, located at the University of Illinois Bondville Field Site. The land inside the triangle is flat to within 5 m, and the elevations of the three sites differ by less than 2 m. Corn (maize) and soybeans were grown in the area, in patches varying from 0.5 to 1 mile (0.8–1.6 km) on a side, with roughly equal proportions of each crop. The crops were in early

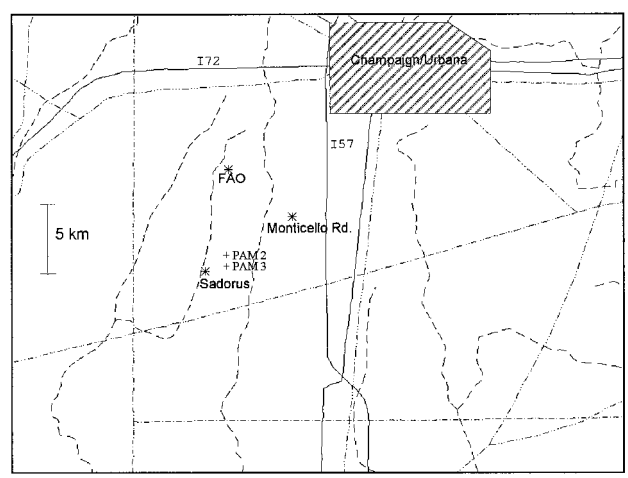

FIG. 1. Map of the experiment region in east-central Illinois. The profiler triangle sites are marked with asterisks and labeled. Two of the Flux-PAM sites are marked with crosses. PAM 1 is not shown for clarity; it was located approximately 0.5 km east of FAO. Roads are shown as solid lines, railroads as dash–double-dot lines, county boundaries as dash–dot lines, and watercourses as dashed lines. Map background courtesy of Xerox PARC World Wide Web Map Server.

stages of development in mid-June, and in fact some of the soybean fields were planted between 15 and 20 June 1996. By 1 August the crops were fully developed, and by 30 September they were fully mature or senescent, with some harvesting taking place in late September. Four to six groups of buildings (farmhouses with outbuildings) per 1 mile (1.6 km) square section were also within the triangle, and the buildings were often surrounded by trees. Narrow gravel or paved roads are on a 1-mile (1.6 km) grid, and a 2-lane highway crosses the northern part of the triangle.

The Flux-PAM systems were located so as to maximize the homogeneous fetch (distance traveled by the air over a uniform surface of interest before reaching the instruments) for as much of the full circle of wind directions as possible. Two of the Flux-PAMs were placed in the centers of adjacent 160-acre (0.8-km^2) fields, one field planted in corn and the other in soybeans, near the southern edge of the triangle. This provided a minimum uniform fetch of 400 m for all wind directions. The third system was placed in a cornfield near FAO and had optimum fetch for southwesterly winds.

The Lidars in Flat Terrain (LIFT) experiment was conducted in conjunction with the later part of Flatland96. Three lidars were located at the Monticello Road field site: a 2-m Doppler lidar (High-Resolution Doppler Lidar) with hemispheric scanner, a high-resolution dual-wavelength backscatter lidar (Scanning/Staring Aerosol Backscatter Lidar) staring vertically, and an ozone Differential Absorption Lidar. An overview of LIFT is provided by S. Cohn et al. (1998, manuscript submitted to *Bull. Amer. Meteor. Soc.*).

2. Instruments and data collected

a. Profilers

The 915-MHz lower-tropospheric wind profiler was developed at the NOAA Aeronomy Lab (Carter et al. 1995; Ecklund et al. 1988). These transportable systems have been deployed at a large number of meteorology and atmospheric chemistry experiments, as well as in long-term studies. A review of some research results from these profilers was presented by Rogers et al. (1993). The wind profiler is a sensitive Doppler radar. Unlike the more familiar weather radars, the profiler is designed to respond to fluctuations of the refractive index in the clear air, although it is also sensitive to particles such as hydrometeors and insects. For the Flatland experiments, the profilers were operated at 60-m vertical resolution with a minimum height of 150 m AGL. Six beam positions, four oblique beams in two coplanar pairs, and two vertical beams of orthogonal polarizations were used. The dwell time on each beam was approximately 25 s. Each cycle also included a single vertical beam measurement at 500-m resolution to detect rain at altitudes up to 12 km. The maximum height of the 60-m resolution measurements varied from 1.5 to 3 km depending on atmospheric conditions, especially humidity, but was always sufficient to cover the convective boundary layer in the summer. Figure 2a shows the height coverage as the fraction of hours with good data at each height for the Monticello Road profiler. There is a slight variation in height coverage among the three months shown, primarily due to differences in humidity. There are no significant differences in the height coverage for 1995 versus 1996, daytime versus nighttime, or from site to site. The wind measurements, when averaged over 30 min, have accuracy and precision better than 1 m s^{-1} (Angevine and MacPherson 1995; Angevine et al. 1998).

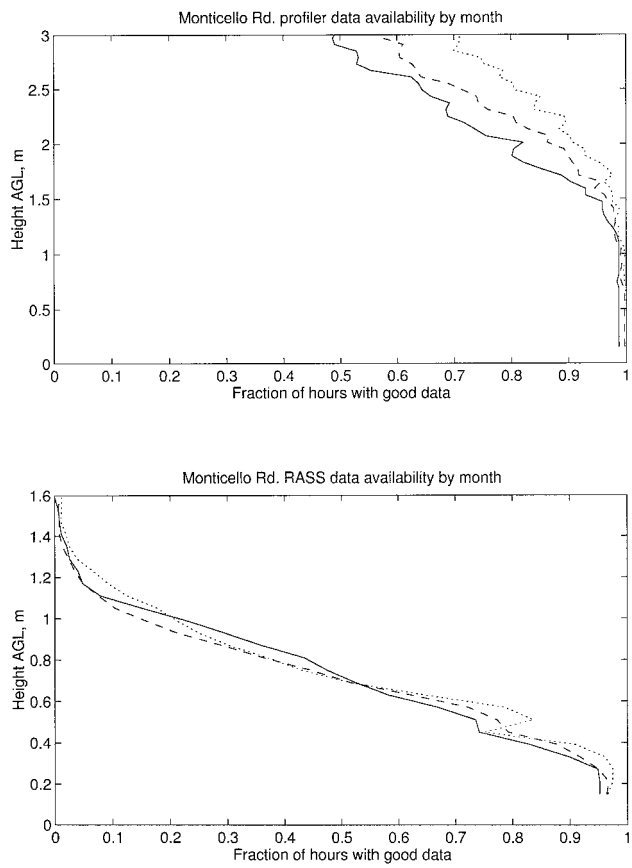

FIG. 2. Monticello Road profiler and RASS data availability during the Flatland96 project. The fraction of possible hours with good data at each height is shown. Availability for June is plotted solid, July dashed, and August dotted.

One of the three profilers in the triangle was the permanently installed system at the FAO. This system has a nine-panel (3 m × 3 m) antenna. The other two profilers were part of Integrated Sounding Systems (ISS) provided by the National Center for Atmospheric Research (NCAR). These systems had four-panel (2 m × 2 m) antennas. All three profilers used the same online control software and hardware and the same operating parameters. In 1996, all three systems had the intermittent contamination removal algorithm ("bird algorithm") (Merritt 1995); in 1995, FAO and Monticello Road had the bird algorithm but the Sadorus system did not. This algorithm is quite helpful in removing intermittent contamination from a variety of objects, particularly birds.

b. RASS

All three profilers were equipped as Radio Acoustic Sounding Systems (RASS) (Angevine et al. 1994b) to measure virtual temperature profiles. An acoustic signal is emitted by four loudspeakers and focusing dishes arranged around the perimeter of the profiler antenna. The profiler measures the speed of sound, and the virtual temperature is derived therefrom. For most of the experiment, the profilers were operated in RASS mode for 3 min every half-hour and the rest of the time in the normal wind mode described above. To avoid disturbing neighbors, neither the Sadorus nor Monticello Road ISS ran in RASS mode at night in 1995, and the Sadorus ISS did not run in RASS mode at night in 1996. Figure 2b shows the height coverage of the Monticello Road ISS in 1996. The other sites and 1995 data have similar coverage. Data are available approximately 50% of the time up to 800 m AGL. The height coverage of RASS at 915 MHz is limited by acoustic attenuation, in addition to the effects of horizontal wind that blows the acoustic energy out of the radar beam. Although the accuracy of RASS is better than 1 K, it is affected by range-dependent biases that are not fully understood (Peters and Angevine 1996). The precision of RASS virtual temperature measurements is approximately 0.5 K (standard deviation) when compared to radiosondes, which of course contribute some of that uncertainty (Angevine and Ecklund 1994).

c. Sondes

Balloon-borne rawinsondes launched from the Sadorus site provided temperature, humidity, and wind data that will be used for budget calculations and for comparisons with the remotely sensed data. We have a high degree of confidence in the winds and boundary layer height information provided by the profilers, but the RASS height coverage is often insufficient to give temperature measurements up to the boundary layer top, and we have no ability to measure humidity remotely. Sondes were launched at 1200 CST every day. On selected "BL intensive" days, sondes were launched at 0900, 1030, 1200, and 1330 CST to map out the boundary layer evolution. Approximately 150 sondes were flown in 1995 and 100 in 1996. The sondes were Vaisala RS-80LH type, and the data were received by the NCAR Cross-chain Loran Atmospheric Sounding System in the Sadorus ISS.

d. Ceilometer

A Vaisala CT-25K laser ceilometer is permanently installed at FAO. It produces estimates of cloud height every 30 s. These estimates are being used in comparisons with the boundary layer height determined from the profiler reflectivity.

e. Flux-PAM

All three Flux-PAMs (Militzer et al. 1995) deployed for Flatland96 determined sensible and latent heat and momentum fluxes at several meters above the canopy. In addition, they measured wind speed and direction at 10 m AGL, temperature and relative humidity at 3 m AGL, pressure, rainfall, net and incoming solar radiation, and soil temperature and heat flux. The Flux-PAM located in the vicinity of the FAO was augmented, having more accurate latent heat flux measurements and ozone deposition flux instrumentation. The Flux-PAMs were fully operational throughout the entire duration of Flatland96.

3. Synoptic and climatological setting

Monthly mean data and deviations from the 1950–95 mean for Illinois Climate Division #5 indicate that Flatland95 occurred during a very hot and somewhat wet August and a cool and very dry September, while Flatland96 took place during a June through August season that started slightly cool and wet and ended up a bit warmer and drier than normal. The following discussion of the synoptic and climatological variability over east-central Illinois during the Flatland experiments is drawn from daily mean data for Champaign, Illinois, provided by the Illinois State Water Survey and from once-daily weather maps published by NOAA's National Centers for Environmental Prediction.

a. Flatland95

A severe heat wave with extremely high humidity occurred in the region in mid-July 1995 (Kunkel et al. 1996; Livezey and Tinker 1996). This was preceded by anomalously high precipitation and flooding, especially south and west of the experiment area (Halpert et al. 1996).

Temperatures in the region were unusually high during August as well (Halpert et al. 1996). August 1995 was the third warmest August on record at Champaign, with a mean temperature of 26.1°C, 3.4°C warmer than average. Clear or hazy skies accompanying high pressure over southern Appalachia or the upper Midwest dominated weather in the Champaign area on 10–14, 21–24, and 26 August. The sky cover was nearly equally split between clear, partly cloudy, and cloudy days, with haze reported on 1 and 14 August. The 136.1 mm of precipitation that fell, 34.0 mm more than average, occurred mostly on 1–4, 7–9, 17, and 19 August in convective events, which were associated with weak frontal boundaries. (On 5–6 August, Tropical Depression Erin moved across southern Illinois to Pennsylvania.) Typical rainfall totals for days with rain were 10–30 mm day^{-1}.

The weather of September 1995 was in sharp contrast to that of the previous month; the 12.7 mm of rainfall, 72.6 mm less than average, made this the seventh driest September on record, and the first frost of the season occurred on 22 September, the first time the temperature in Champaign had dipped below freezing during September since 1961. The mean temperature for the month was 17.6°C, 1.6°C less than average. Clear skies and propagating ridges of high pressure dominated Champaign-area weather on 1–3, 17–18, 23, and 26–28 September. Skies were clear, partly cloudy, and cloudy in equal measure during the month. The mean wind was from the southeast at 1.9 m s^{-1}, but the daily mean winds were bimodially distributed about the north and southeast directions. This reflects the very autumnlike sequence of low pressure systems that developed in the Midwest and moved through Illinois during September. Precipitation never exceeded 10.0 mm day^{-1} and usually fell in association with developing surface lows passing through the state, although the precipitation on 6–7 September was predominantly convective, while that on 19 and 21 September was stratiform.

b. Flatland96

With a monthly mean temperature of 21.9°C, June 1996 was only 0.3°C cooler than normal. Skies were clear on 5 June under a broad ridge of high pressure centered over Illinois and Kentucky. A high moving southeastward from the Great Lakes region to Tennesee and North Carolina on 25–29 June brought mostly clear skies and some haze to the Champaign area. Cloudy skies were reported on 14 days and clear skies on only 8, with haze being reported on 28–30 June. The 143.5 mm of rain that fell at Champaign, 61 mm of it on 16 June, were 40.1 mm greater than average. Rain fell on 1–3, 6, 8–10, 16, 17, and 22–24 June. The rain was both stratiform and convective, and often fell in association with a combination of a nearby stationary front and a surface low developing underneath upper-level shortwaves.

July 1996 in Champaign was cool (22.3°C, 1.6°C cooler than average) with a record low maximum recorded on 21 July. High pressure centered in the midwest and the Ohio Valley produced clear skies in the Champaign area on 3, 5, and 10–11 July. Skies were partly cloudy 40% of the time and cloudy another 40% of the time, no doubt accounting for some of the low daily-mean temperatures. It was also dry, with 85.3 mm of rain (28.4 mm less than average), even though measureable precipitation was recorded on 9, 14, 16, 21, 23, 24, 28, and 30–31 July. Rainfall was mostly convective and light (less than 10 mm day^{-1}), although 41 mm fell on 21 July. Rain was often associated with the passage of a cold front trailing from a surface low over the Great Lakes or southern Canada.

Champaign temperatures returned to near normal in August, with the mean of 23.2°C being 0.6°C warmer than average. However, this was the ninth driest August on record, with 36.1 mm of rain, 66.0 mm less than average. A series of high pressure systems, usually propagating southeastward from the upper Midwest and Great Plains, brought clear skies to Champaign on 1, 3, 10, 13, 24–25, and 28–31 August. Clear skies on 60% of the days of August contributed to the slightly warm and very dry conditions; haze was reported only on 4 August. Measureable precipitation, which fell on 17, 18, 23, 26, and 27 August, was mostly from convection associated with weak fronts and was always less than 15 mm day^{-1}. The mean wind was from the northeast at 1.5 m s^{-1}.

4. Preliminary results

In this section, we present some preliminary results of the experiments, both in statistical form and as case studies. Data analysis is continuing, and we expect to

report detailed results related to the objectives described above at later times.

a. Example cases

We have selected six example days to show the range of boundary layer phenomena observed during the two experiment campaigns. These examples also serve to introduce the profiler's ability to measure boundary layer height and structure to those who may not be familiar with it. The first example is day 228 (16 August) 1995, shown in Fig. 3. The series of soundings show a fairly well-defined convective boundary layer developing through the morning hours, with a somewhat weak inversion above. Surface and near-surface humidity is very high and rises through the day. Winds in the boundary layer (BL) (not shown) were 6–8 m s^{-1} from the south, with southwesterly winds above the BL.

The top of a convective boundary layer is present as a distinctive signature in a time–height plot of profiler reflectivity. Generally, a strong peak of reflectivity is seen at the boundary layer top, although the strength of this peak depends on a variety of factors. The reflectivity peak is the result of strong gradients of temperature and especially humidity. Such gradients, although not usually as strong, may also be present at the boundaries of other atmospheric layers. The lower panel of Fig. 3 shows the reflectivity (range-corrected signal-to-noise ratio) measured by all beams of the profiler. The profiler is not calibrated, so the reflectivity is presented on an arbitrary scale. No averaging has been done, so the time resolution is about 30 s. The boundary layer top can be seen rising from approximately 500 m AGL at 0900 CST to about 1000 m at 1300 CST. Structure in the entrainment zone due to rising thermals and sinking downdrafts is quite visible throughout the morning. As deep clouds appeared after 1300 CST (cloud altitudes found by the ceilometer are shown as crosses), the reflectivity signature of the BL top became less clear.

The solid green line in the lower panel of Fig. 3 is the boundary layer height determined by an automatic algorithm (Angevine et al. 1994a) that finds the peak of the reflectivity in each vertical profile, then takes the median of those peaks over an hour as the BL top. The algorithm was run every half hour, so the points are the hourly average BL height on a half-hour grid.

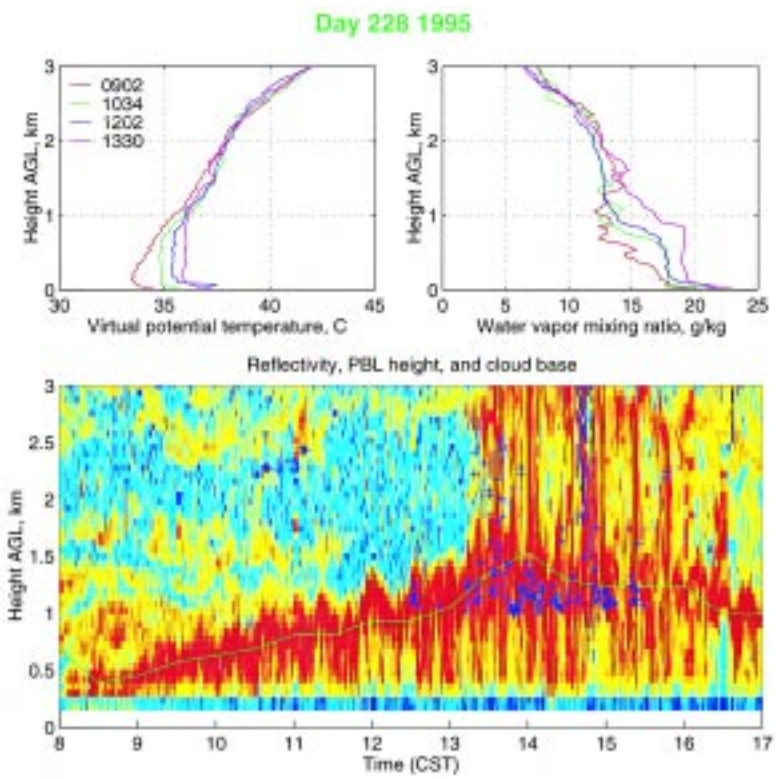

FIG. 3. Case example of day 228 (16 August) 1995. Virtual potential temperature and water vapor mixing ratio from four soundings at the times shown are plotted in the upper panels. The lower panel shows the profiler reflectivity (arbitrary scale) in pseudocolor. The solid green line is the automatically determined boundary layer height, and the blue crosses are cloud-base heights detected by the ceilometer.

Day 253 (10 September) 1995 shows a quite different boundary layer structure (Fig. 4). The 0905 sounding shows a shallow boundary layer and a 1500-m-deep residual layer, which is also visible in the reflectivity plot. Surface and BL humidities were much lower than on day 228 and changed little during the day. The BL top, as shown by the reflectivity plot, grew rapidly into the residual layer between 0930 and 1130 and was then prevented from significant further growth by the very strong and sharp capping inversion. A few shallow clouds formed between 1100 and 1230 CST. The winds in and above the BL were 6–8 m s^{-1} from the northeast.

Day 266 (23 September) 1995 had yet another type of boundary layer structure and evolution (Fig. 5). The capping inversion was still strong, and the surface, boundary layer, and overlying atmosphere were very dry. No clouds were

present. Boundary layer growth was gradual and steady through the day. Structure in the entrainment zone can again be seen in the reflectivity plot. Boundary layer winds were 2–5 m s^{-1} from the east.

In 1996, the experiment was conducted earlier in the year (15 June–23 September). Figure 6 shows the example of day 207 (25 July). The boundary layer structure on this day was similar to that on day 228 of 1995 (Fig. 3) but drier and deeper. The capping inversion was weak, leading to development of clouds with significant vertical extent. Winds in the BL were 6–8 m s^{-1} from the west, with slightly stronger winds from the same direction above the BL. The failure of the automatic boundary layer height finding algorithm in the late afternoon is not surprising since it is difficult to define the boundary layer top either theoretically or from measurements when deep clouds are present. The main surface energy budget terms measured by Flux-PAM #1 at the FAO are shown in the bottom panel of this and the other examples from 1996. The net radiation was strongly influenced by the clouds. The latent heat flux was considerably higher than the sensible heat flux.

Plots for day 218 (5 August) 1996 are shown in Fig. 7. The reflectivity plot and the soundings show strong humidity gradient structure in the free troposphere above the BL, which grew steadily through the day until about 1400 CST. The surface and BL were very warm and humid. The latent heat flux dominated over the sensible heat flux at the surface. Only a few clouds were detected. Boundary layer winds were 8–10 m s^{-1} from the south, with winds above the BL from the southwest.

The next day, day 219 (6 August) 1996, shown in Fig. 8, had a similar structure to day 253 1995 (Fig. 4), but day 219 1996 was much warmer and more humid. The boundary layer grew rapidly between 0930 and 1030 CST into a residual layer and then grew more

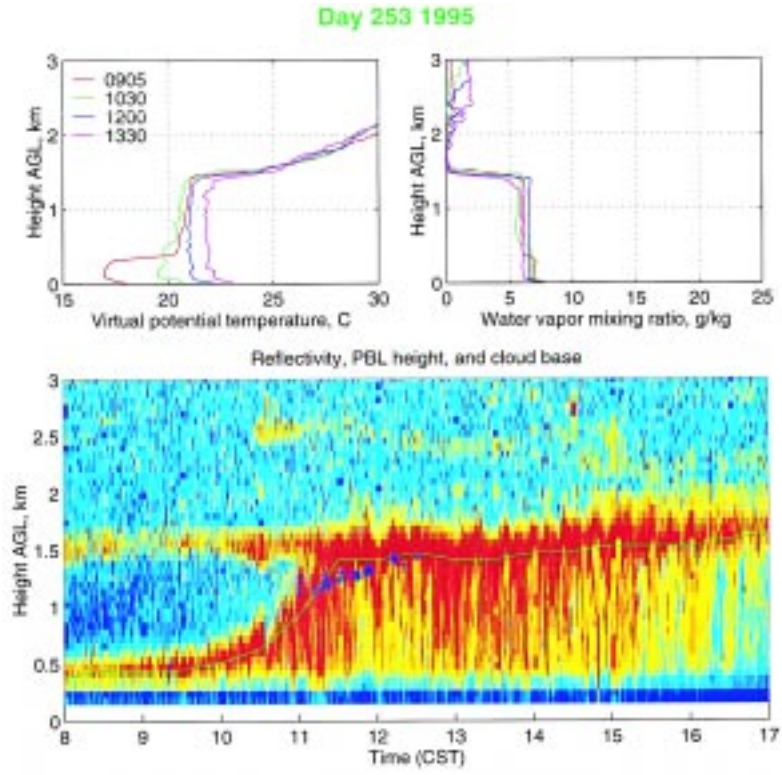

FIG. 4. Case example of day 253 (10 September) 1995. Plotting conventions as in Fig. 3.

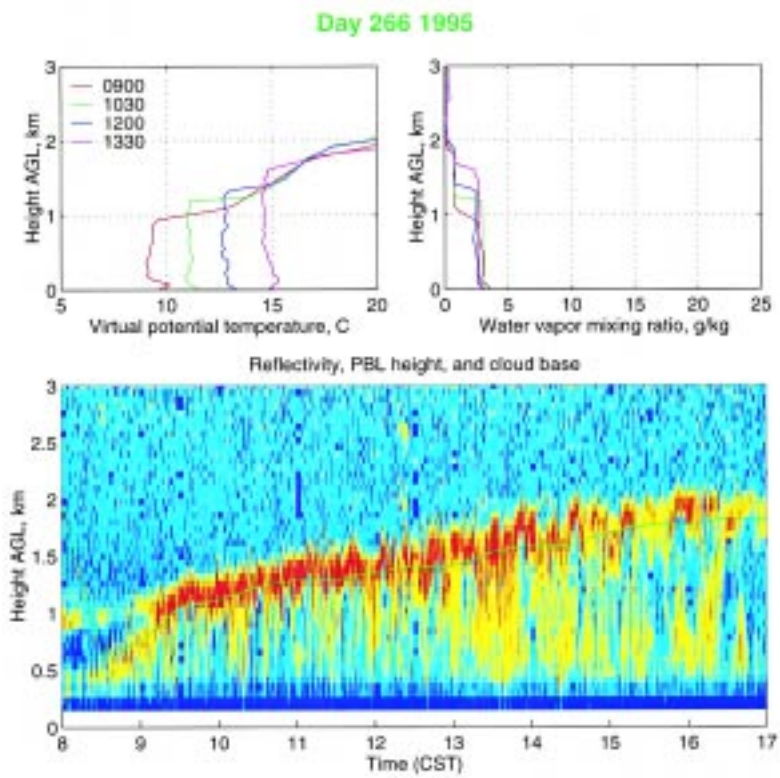

FIG. 5. Case example of day 266 (23 September) 1995. Plotting conventions as in Fig. 3.

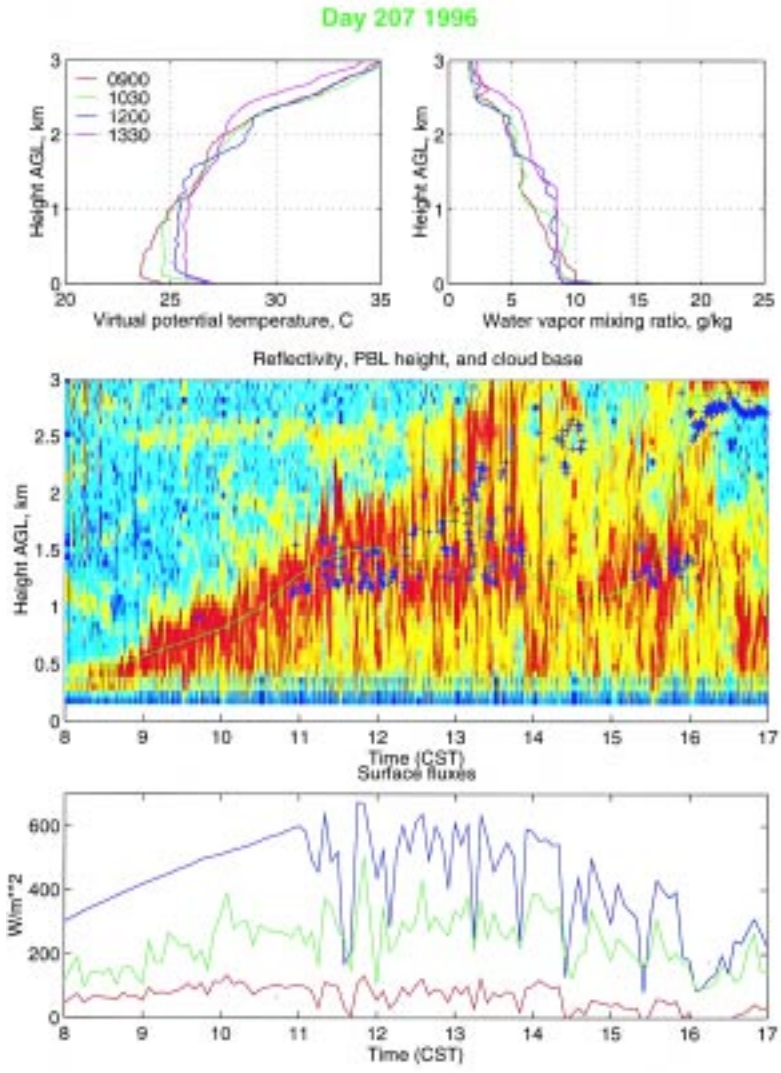

FIG. 6. Case example of day 207 (25 July) 1996. Plotting conventions as in Fig. 3. Bottom panel shows net solar radiation (upper trace, magenta), latent heat flux (middle trace, green), and sensible heat flux (lower trace, red) measured by PAM 1.

slowly, restrained by a moderately strong capping inversion. A few shallow clouds were detected, but they have little effect on the reflectivity structure. The latent heat flux again dominated the surface energy budget. Boundary larger winds were 6–8 m s^{-1} from the south to southwest.

b. Winds

Figures 9 and 10 show statistics of the daytime boundary layer winds for the two campaigns. These are averages of winds from all three profilers over all heights within the connective boundary layer. In August and September 1995 (Fig. 9), the wind direction in the boundary layer was most often from the southwest, less often from the north and northeast, and only rarely from the southeast or northwest. The southwest quadrant predominated more strongly at the surface (not shown). The boundary layer wind speed distribution was sharply peaked at approximately 5 m s^{-1}, with speeds over 10 m s^{-1} occurring only rarely. Surface wind speeds were (not surprisingly) lighter, with a median of approximately 3 m s^{-1}. Median boundary layer wind speeds (not shown) were strongest in the northwest and southwest quadrants.

In contrast, the boundary layer winds for 15 June–23 August 1996 (Fig. 10) were more often from the northwest, fairly often from the southwest, and only rarely had any easterly component. The surface wind directions had much the same distribution. Boundary layer wind speeds were more broadly distributed in 1996, although the median speed is only slightly higher. The same is true at the surface. Median boundary layer wind speeds were highest in the southwest quadrant.

c. Temperature, humidity, pressure, and rainfall

Figure 11 shows the temperature, humidity, and barometric pressure traces at the FAO site for the 1995 campaign. As previously noted for the region in general, August was unusually hot and very humid, with water vapor mixing ratios well over 20 g kg^{-1} at the surface during the day on days 220–232 (8–20 August). On day 243 (31 August), the humidity dropped sharply. The mixing ratio and its diurnal cycle were both sharply reduced for the remainder of the experiment. This was probably due both to a change in the synoptic regime (see section 3a above) and to the maturing of the crops and consequent cessation of evapotranspiration. No measurable rain fell between 20 August and 7 September, so soil moisture was probably quite low. In 1995, measurable rain fell at FAO on 3, 4, 7, 9, 10, 17, and 19 August and 7, 8, 20, and 21 September.

The 1996 experiment occurred earlier in the season and in a less unusual year. The temperature, hu-

midity, and pressure traces from the Flux-PAM installation at the FAO site are shown in Fig. 12. Humidities were more moderate than in 1995, only a few days showing mixing ratios higher than 20 g kg^{-1}. Measurable rain fell at FAO on 16, 17, and 23 June, 14, 16, 21, 24, 28, 29, and 30 July, and 17–18 August.

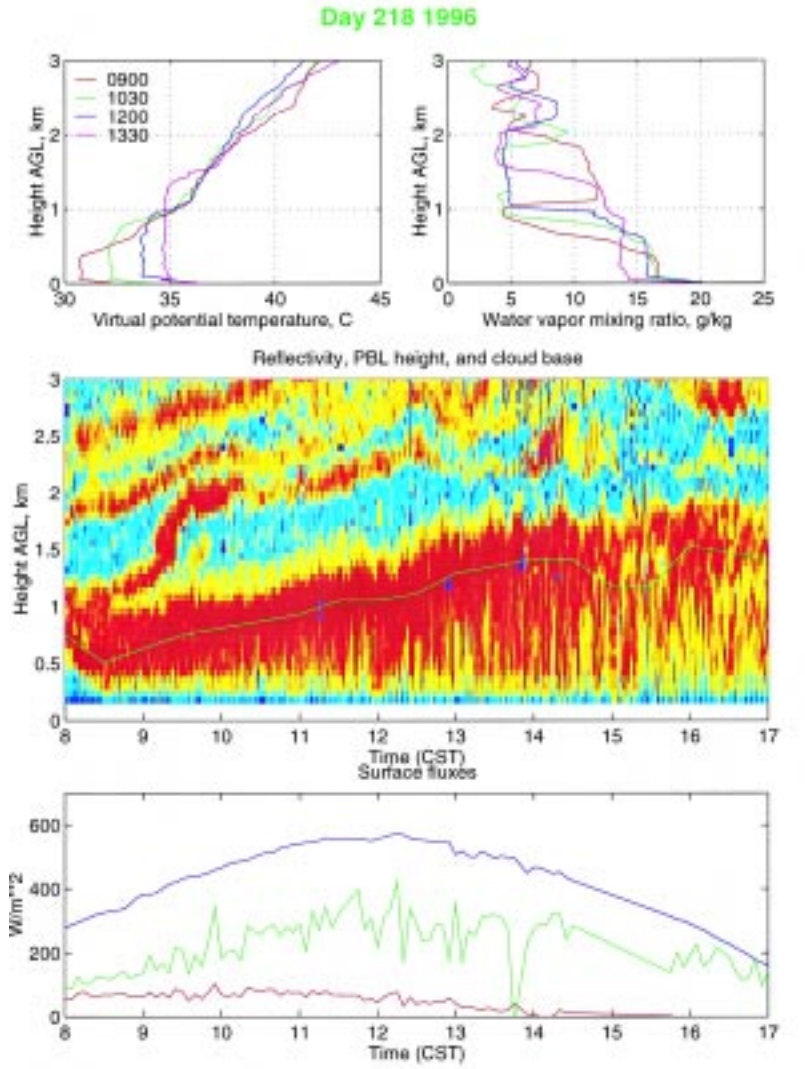

FIG. 7. Case example of day 218 (5 August) 1996. Plotting conventions as in Fig. 6.

d. Boundary layer height

As shown in the case examples above, the profiler can measure the height of the convective boundary layer (Angevine et al. 1994a), also variously described as the mixing depth or boundary layer depth. The boundary layer top is indicated by a peak in the profiler reflectivity, primarily due to the humidity gradient present there. Humidity gradients due to other types of layering also are frequently visible, as in Figs. 4 and 7. This can be useful in studies of other types of boundary layers (White et al. 1991; Rogers et al. 1993; Angevine et al. 1996). Figure 13 shows the midday boundary layer height for all days with well-formed convective boundary layers in the two experiment periods. The height shown for each day is the average over three hours in early afternoon (1200–1500 CST) of the boundary layer heights determined for each hour by subjective examination of the results of a peak-finding algorithm run on the reflectivity from two (1995) or all three (1996) profilers. Only two profilers were included in the 1995 results because the third profiler was not running the bird algorithm and its reflectivity results were considered less reliable.

The boundary layer height is determined by a variety of factors and is not simply related to any local surface meteorological variables, but we can see some broad relationships. In Fig. 13a, the consistent low boundary layer heights for days 220–235 (8–23 August) 1995 are probably related to low Bowen ratios (ratio of sensible to latent heat flux at the surface) and very high humidities as discussed above. Most of the net solar radiation evaporated moisture rather than heating the surface, and therefore contributed little to buoyant forcing. Subsidence due to high pressure probably also contributed. Days with rain are excluded from the dataset since the profiler cannot measure BL heights in rain. With a few exceptions, the drier period in September has higher boundary layers.

e. Surface fluxes

The three Flux-PAM stations deployed in 1996 measured all components of the surface energy balance in two fields of corn (maize) and one of soybeans. For both crops, the incoming solar radiation was partitioned into more latent than sensible heat flux. The Bowen was approximately 0.4 when averaged over all days with good flux data and over daytime hours (0800–1700 CST). Figure 14 shows the Bowen ratio for each day of the 1996 campaign on which the Krypton hygrometer was operating. The Bowen ratio was generally higher (proportionally more sensible heat

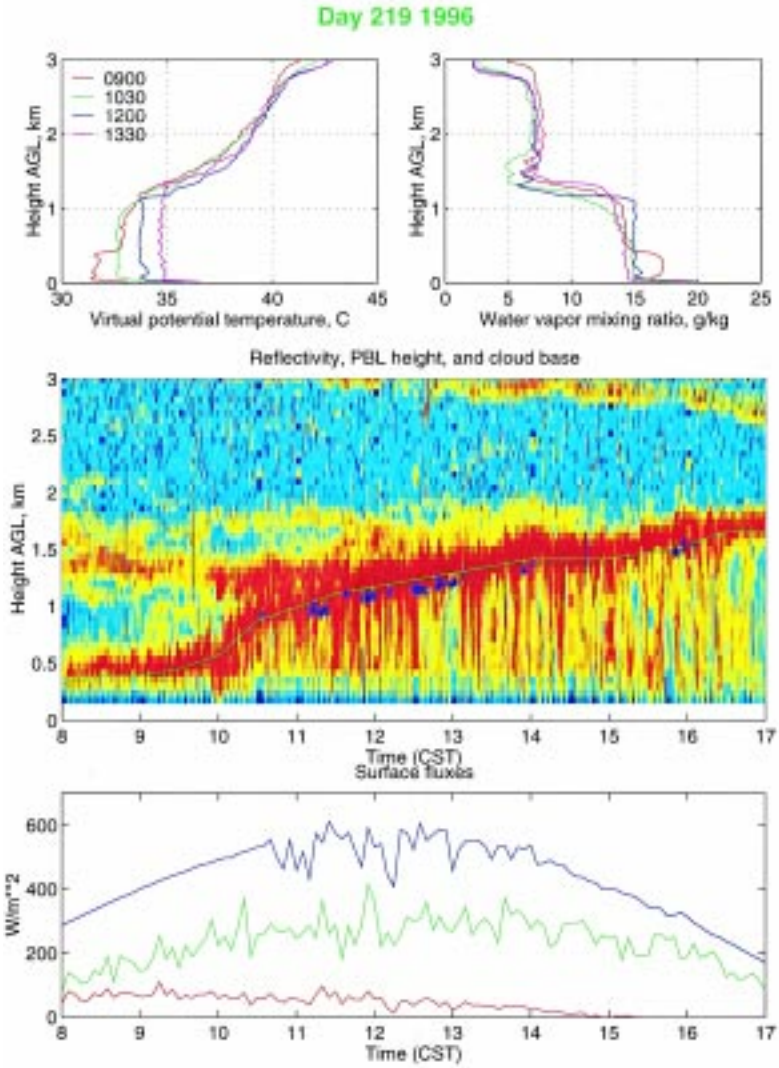

FIG. 8. Case example of day 219 (6 August) 1996. Plotting conventions as in Fig. 6.

flux) early and late in the campaign and lower (proportionally more latent heat flux) in the middle.

There were some significant differences in the surface fluxes observed at the three sites, although these had more to do with the state of maturity of the crop than with the crop type. Figure 15 shows the surface virtual temperature flux for site 2 (corn) and site 3 (soybeans) for the noon hour each day. The soybeans at site 3 were planted late and bare soil was exposed until mid-July. The surface fluxes at this site depended much more strongly and immediately on recent rainfall than the fluxes at sites 1 and 2, which had much more leaf area throughout.

5. Summary

In this article, we have described the objectives and instruments used in the Flatland boundary layer experiments Flatland95 and Flatland96. We have also described the synoptic and climatological setting and shown examples of the data in the form of cases as well as statistics. The data from these experiments will be useful in exploring convective boundary layer behavior, especially the behavior of the entrainment zone, and in refining techniques for use of wind-profiling radars in boundary layer studies.

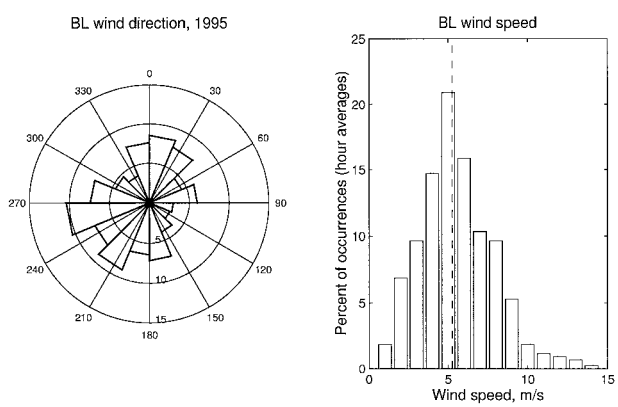

FIG. 9. Boundary layer wind speed and direction statistics for Flatland95 project. Wind rose shows percent occurrences in each 22.5° bin, outermost ring is 15%. Dashed vertical line is median speed.

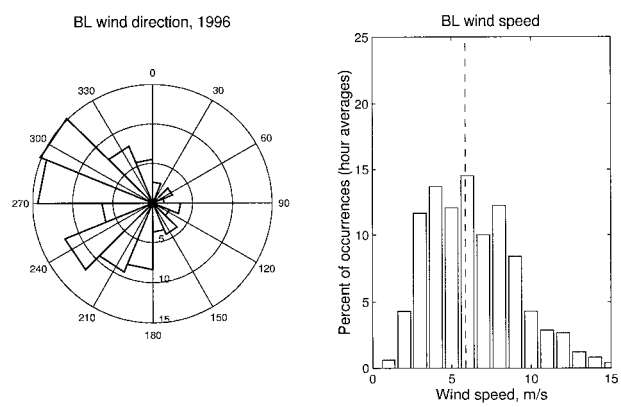

FIG. 10. Boundary layer wind speed and direction statistics for Flatland96 project. Plotting conventions as in Fig. 9.

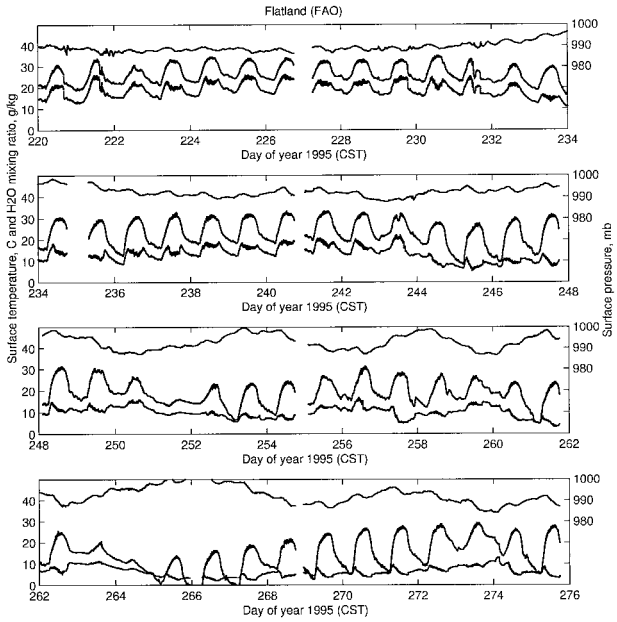

FIG. 11. Surface barometric pressure (upper trace, right-hand scale), temperature (middle trace, left-hand scale), and water vapor mixing ratio (lower trace, left-hand scale) measured by the surface meteorological instruments at FAO for the entire Flatland95 campaign.

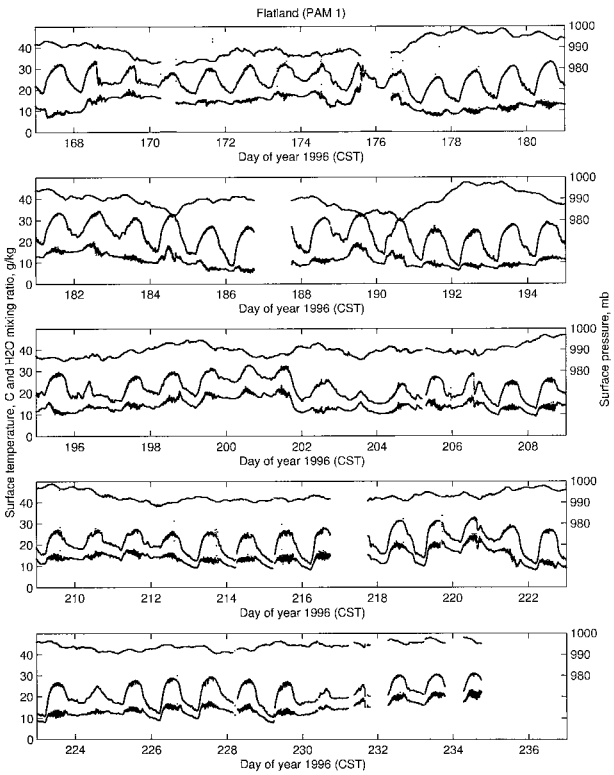

FIG. 12. As Fig. 11 for measurements from PAM 1 for Flatland96 campaign.

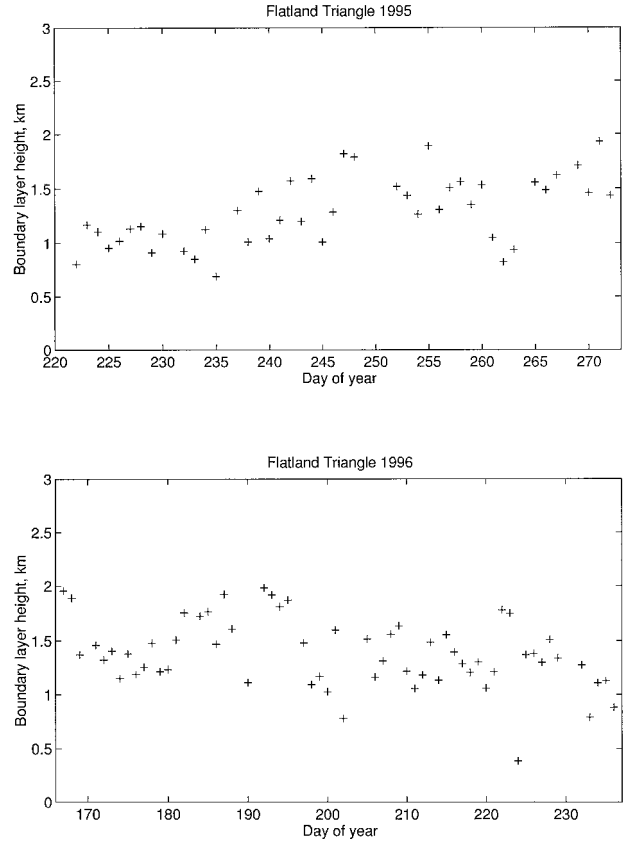

FIG. 13. Boundary layer heights from profiler measurements found by a hybrid objective and subjective technique. Heights shown are the average over 1200–1500 CST for each day: (top) 1995; (bottom) 1996.

One of the instrumental objectives has already been met. Angevine (1997) describes errors in the mean vertical velocities measure by the vertical beam of the boundary layer profiler. These directly measured vertical velocities are 0.1–0.3 m s^{-1} downward in daytime, with a distinct diurnal cycle and vertical profile. The vertical velocities calculated from the divergence of the horizontal wind measured by the profiler triangle, which are not significantly different from zero over long time averages, were used to determine that the directly measured velocities are erroneous. Measurements of fluctuating components of vertical velocity are not affected because the fluctuating components are very much larger in magnitude. The errors in the mean vertical velocities are probably due to particulate scatterers such as insects or hydrometeors.

Acknowledgments. The Flatland Atmospheric Observatory and this project are supported by the National Science Foundation under Grant ATM-9419638. The Integrated Sounding Sys-

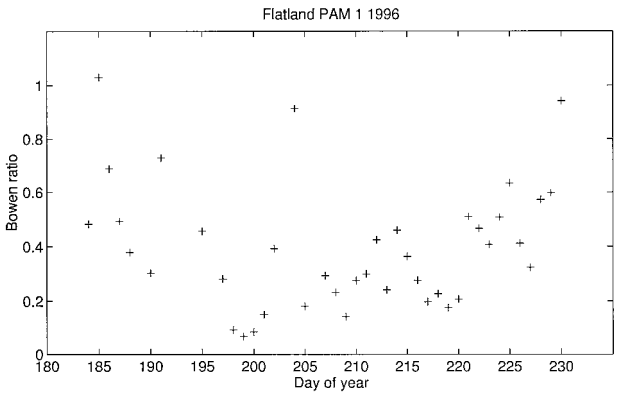

FIG. 14. Bowen ratio (sensible heat flux/latent heat flux) from PAM 1 for Flatland96. Ratios shown are the average over 0800–1700 CST for each day.

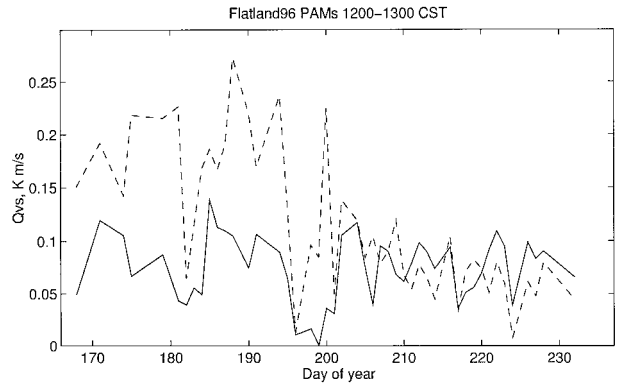

FIG. 15. Surface virtual temperature flux from PAM sites 2 (solid) and 3 (dashed) for 1200–1300 CST on each day with good data.

tems (ISS) and Flux-PAMs were provided by the National Center for Atmospheric Research Surface and Sounding Systems Facility. The ISS were installed and operated by Michael Susedik, Stephen Cohn, Carmen Paneitz, Harold Cole, James Owens, and Lou Verstraete. Flux-PAM personnel were Steve Oncley, John Militzer, Tom Horst, Kurt Knudson, Charlie Martin, Matt Michaelis, and Santiago Newbery. The FAO and Monticello Road sites were provided by the University of Illinois Department of Electrical Engineering, with site selection help from Dr. Steven Franke, Dr. James Coleman, and Dr. Erhan Kudeki. Stanley Henson of the University of Illinois operates and maintains the FAO. One of the authors (LMH) was supported by the NOAA Office of Global Programs through grants to the NOAA Aeronomy Laboratory. The Champaign, Illinois, climatological data were provided by Steve Hilberg of the Illinois State Water Survey. Climatological data from Illinois Climate Division 05 are from the National Climate Data Center climate division dataset and the NOAA Climate Diagnostics Center. Mention of a commercial company or product does not constitute an endorsement by NOAA/ERL. Use of information from this publication concerning proprietary products or the tests of such products for publicity or advertising purposes is not authorized.

References

Angevine, W. M., 1997: Errors in mean vertical velocities measured by boundary layer wind profilers. *J. Atmos. Oceanic Technol.,* **14,** 565–569.

——, and W. L. Ecklund, 1994: Errors in radio acoustic sounding of temperature. *J. Atmos. Oceanic Technol.,* **11,** 837–848.

——, and J. I. MacPherson, 1995: Comparison of wind profiler and aircraft wind measurements at Chebogue Point, Nova Scotia. *J. Atmos. Oceanic Technol.,* **12,** 421–426.

——, A. B. White, and S. K. Avery, 1994a: Boundary layer depth and entrainment zone characterization with a boundary layer profiler. *Bound.-Layer Meteor.,* **68,** 375–385.

——, W. L. Ecklund, D. A. Carter, K. S. Gage, and K. P. Moran, 1994b: Improved radio-acoustic sounding techniques. *J. Atmos. Oceanic Technol.,* **11,** 42–49.

——, and Coauthors, 1996: Local meteorological features affecting chemical measurements at a North Atlantic coastal site. *J. Geophys. Res.,* **101,** 28 935–28 946.

——, P. S. Bakwin, and K. J. Davis, 1998: Wind profiler and RASS measurements compared with measurements from a 450 m tall tower. *J. Atmos. Oceanic Technol.,* in press.

Barr, A. G., and A. K. Betts, 1998: Radiosonde boundary-layer budgets above a boreal forest. *J. Geophys. Res.,* in press.

Betts, A. K., and A. G. Barr, 1996: First international satellite land surface climatology field experiment 1987 sonde budget revisited. *J. Geophys. Res.,* **101,** 23 285–23 288.

——, R. L. Desjardins, and J. I. MacPherson, 1992: Budget analysis of the boundary layer grid flights during FIFE 1987. *J. Geophys. Res.,* **97,** 18 533–18 546.

Carter, D. A., K. S. Gage, W. L. Ecklund, W. M. Angevine, P. E. Johnston, A. C. Riddle, J. Wilson, and C. R. Williams, 1995: Developments in UHF lower tropospheric wind profiling at NOAA's Aeronomy Laboratory. *Radio Sci.,* **30,** 977–1001.

Davis, K. J., D. H. Lenschow, S. P. Oncley, C. Kiemle, G. Ehret, A. Giez, and J. Mann, 1998: The role of entrainment in surface–atmosphere interactions over the boreal forest. *J. Geophys. Res.,* in press.

Ecklund, W. L., D. A. Carter, and B. B. Balsley, 1988: A UHF wind profiler for the boundary layer: Brief description and initial results. *J. Atmos. Oceanic Technol.,* **5,** 432–441.

Grossman, R. L., 1992: Convective boundary layer budgets of moisture and sensible heat over an unstressed prairie. *J. Geophys. Res.,* **97,** 18 425–18 438.

Halpert, M. S., G. D. Bell, V. E. Kousky, and C. F. Ropelewski, 1996: Climate Assessment for 1995. *Bull. Amer. Meteor. Soc.,* **77,** S1–S44.

Kunkel, K. E., S. A. Changnon, B. C. Reinke, and R. W. Arritt, 1996: The July 1995 heat wave in the Midwest: A climatic perspective and critical weather factors. *Bull. Amer. Meteor. Soc.,* **77,** 1507–1518.

Livezey, R. E., and R. Tinker, 1996: Some meteorological, climatological, and microclimatological considerations of the severe U.S. heat wave of mid-July 1995. *Bull. Amer. Meteor. Soc.,* **77,** 2043–2054.

Merritt, D. A., 1995: A statistical averaging method for wind profiler Doppler spectra. *J. Atmos. Oceanic Technol.,* **12,** 985–995.

Militzer, J. M., M. C. Michaelis, S. R. Semmer, K. S. Norris, T. W. Horst, S. P. Oncley, A. C. Delany, and F. V. Brock, 1995: Development of the prototype PAMIII/Flux-PAM surface meteorological station. *Preprints, Ninth Symp. on Meteorological Observations and Insturmentation,* Charlotte, NC, Amer. Meteor. Soc., 490–494.

Peters, G., and W. M. Angevine, 1996: On the correction of RASS-temperature errors due to turbulence. *Contrib. Atmos. Phys.*, **69,** 81–96.

Rogers, R. R., W. L. Ecklund, D. A. Carter, K. S. Gage, and S. A. Ethier, 1993: Research applications of a boundary-layer wind profiler. *Bull. Amer. Meteor. Soc.*, **74,** 567–580.

Stull, R. B., 1988: *An Introduction to Boundary Layer Meteorology.* Kluwer Academic, 666 pp.

Trainer, M., B. A. Ridley, M. P. Buhr, G. Kok, J. Walega, G. Hübler, D. D. Parrish, and F. C. Fehsenfeld, 1995: Regional ozone and urban plumes in the southeastern United States: Birmingham, a case study. *J. Geophys. Res.*, **100,** 18 823–18 834.

White, A. B., C. W. Fairall, and D. W. Thomson, 1991: Radar observations of humidity variability in and above the marine atmospheric boundary layer. *J. Atmos. Oceanic Technol.*, **8,** 639–658.

Young, P. W., and E. W. Eloranta, 1995: Calculation of divergence and vertical motion from volume imaging lidar data. *J. Geophys. Res.*, **100,** 25 577–25 583.